Supporting Information: Thermodynamic Driving Forces of Guest Confinement in a Photoswitchable Cage

Selina Juber,[†] Sebastian Wingbermühle,[†] Patrick Nuernberger,[‡] Guido H. Clever,[¶] and Lars V. Schäfer[*,†]

[†]*Theoretical Chemistry, Ruhr University Bochum, 44780 Bochum, Germany*

[‡]*Institut für Physikalische und Theoretische Chemie, Universität Regensburg, 93040 Regensburg, Germany*

[¶]*Department of Chemistry, TU Dortmund University, 44227 Dortmund, Germany*

E-mail: lars.schaefer@ruhr-uni-bochum.de

1. Force field parameters and validation

Table S1: Atomic partial charges for the isolated DTE ligands and for the cages. See Figure S1 for atom numbers.

Nr.	Ligand open	Ligand closed	Cage open	Cage closed
Pd	–	–	0.50	0.50
C2	-0.09	-0.11	-0.06	-0.08
C3	0.41	0.42	0.45	0.47
H4	0.02	0.03	0.02	0.03
N5	-0.66	-0.66	-0.53	-0.54
C6	0.40	0.41	0.44	0.45
H7	0.02	0.02	0.02	0.02
C8	-0.24	-0.24	-0.19	-0.20
H9	0.14	0.15	0.14	0.14
C10	-0.06	-0.06	-0.03	-0.02
H11	0.14	0.14	0.14	0.14
C12	-0.08	-0.04	-0.08	-0.02
C13	-0.07	-0.05	-0.05	-0.03
C14	-0.01	0.08	-0.00	0.09
S15	0.08	-0.16	0.10	-0.15
C16	-0.10	-0.16	-0.10	-0.15
H17	0.17	0.17	0.17	0.17
C18	-0.11	0.00	-0.10	0.01
C19	-0.11	0.00	-0.10	0.01
C20	-0.01	0.08	-0.00	0.09
S21	0.08	-0.16	0.10	-0.15
C22	-0.02	-0.14	-0.02	-0.13

C23	-0.10	-0.16	-0.09	-0.15
H24	0.17	0.17	0.17	0.17
C25	-0.02	-0.14	-0.02	-0.13
C26	-0.06	0.06	-0.04	0.05
C27	-0.04	-0.09	-0.06	-0.09
H28	0.06	0.06	0.06	0.06
H29	0.06	0.06	0.06	0.06
H30	0.06	0.06	0.06	0.06
C31	-0.06	0.06	-0.04	0.05
C32	-0.04	-0.09	-0.04	-0.08
H33	0.06	0.06	0.06	0.06
H34	0.06	0.06	0.06	0.06
H35	0.06	0.06	0.06	0.06
C36	0.42	0.44	0.42	0.44
F37	-0.20	-0.20	-0.19	-0.20
F38	-0.20	-0.20	-0.20	-0.19
C39	0.32	0.33	0.31	0.33
F40	-0.19	-0.19	-0.19	-0.18
F41	-0.19	-0.19	-0.19	-0.18
C42	0.42	0.44	0.42	0.44
F43	-0.20	-0.20	-0.21	-0.20
F44	-0.20	-0.20	-0.19	-0.19
C45	-0.07	-0.05	-0.06	-0.03
C46	-0.08	-0.04	-0.08	-0.04
C47	-0.09	-0.11	-0.06	-0.08
C48	0.41	0.42	0.45	0.47

H49	0.02	0.03	0.02	0.03
N50	-0.66	-0.66	-0.53	-0.54
C51	0.40	0.41	0.44	0.45
H52	0.02	0.02	0.02	0.02
C53	-0.24	-0.24	-0.19	-0.20
H54	0.14	0.15	0.14	0.14
C55	-0.06	-0.06	-0.03	-0.02
H56	0.14	0.14	0.14	0.14

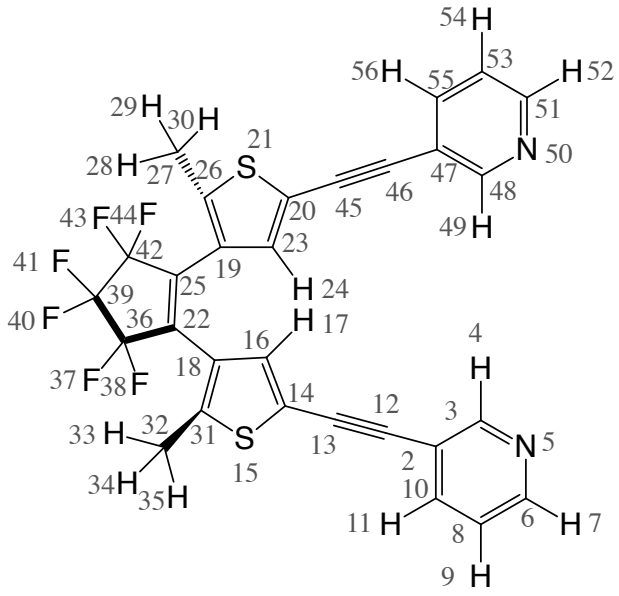

Figure S1: Labeled atoms in the DTE ligand, as referred to in Table S1.

A Morse potential (equation 1) was used for the N-Pd bond in the force field. The force field parameters were fitted to the B3LYP potential energy curve. This resulted in values of 16.295 nm^{-1} for β, 0.205 nm for r_e and 228.104 $kJ\,mol^{-1}$ for D_e in Eq. 1. The curves are

shown in Figure S2.

$$V(r) = D_{\mathrm{e}}(1 - e^{-\beta(r-r_{\mathrm{e}})})^2 \tag{1}$$

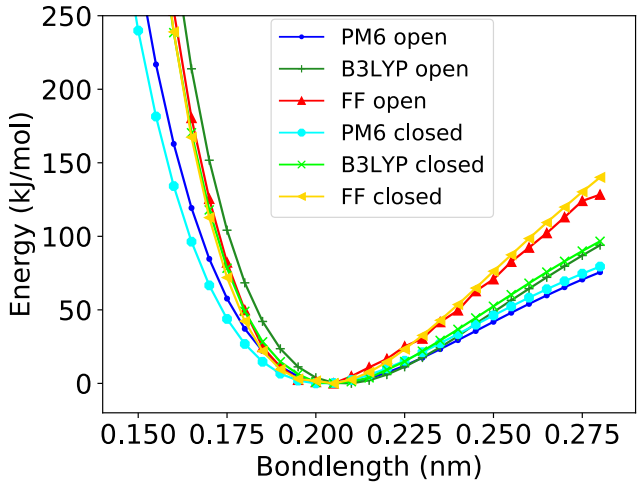

Figure S2: Relaxed potential energy surface scan of the N-Pd bond in the cage.

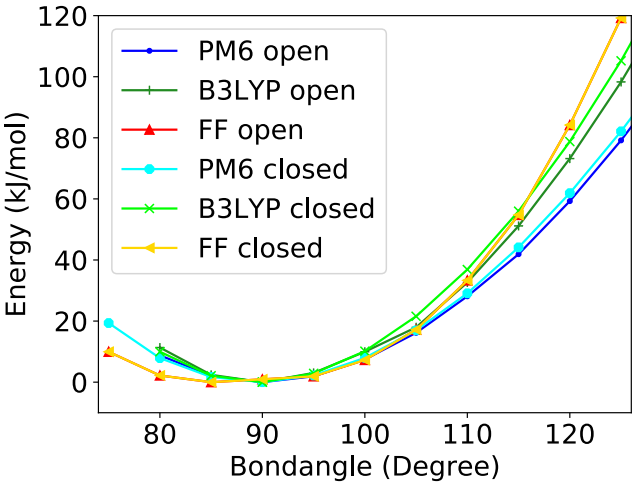

Figure S3: Relaxed potential energy surface scan of the N-Pd-N angle in the cage.

For the potential of the N-Pd-N angle the curves show a harmonic form, which is why a harmonic potential (see Figure S3) was fitted to describe the angles in the force field. The resulting angle force constant is 339.4 kJ mol^{-1} rad^{-2}.

For the final parameter set, the performance of the force field was tested in terms of its ability to describe the structure and energetics of the system.

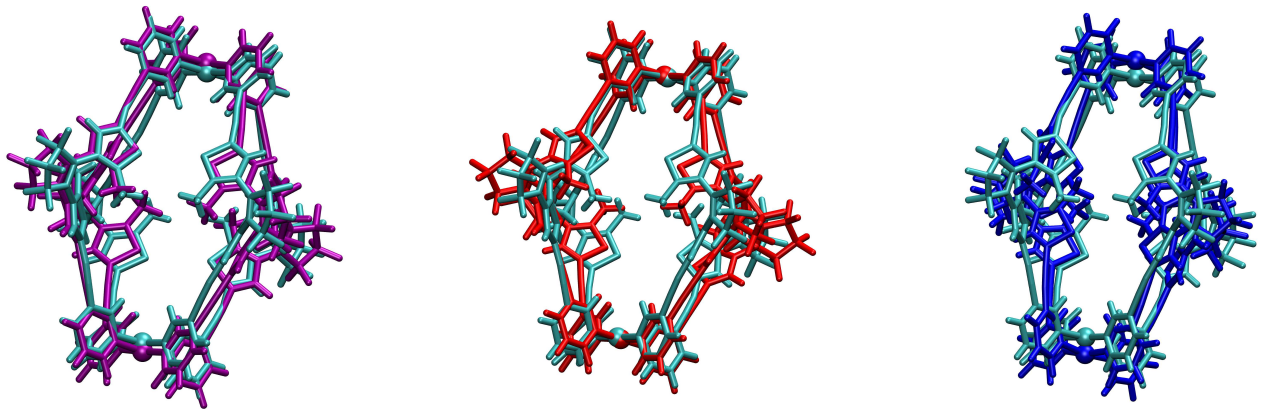

Figure S4: Superimposition of the X-ray crystal structure (cyan) with the B3LYP/6-31G* optimized cage structure (indigo), the PM6 optimized cage (red), and the structure of the cage obtained with the force field (blue).

Figure S4 shows the structural alignments. RMSD calculation of the B3LYP/6-31G*, PM6, and force field optimized structures with respect to the crystal structure of the open cage yield all-atom RMSD values of 0.11 nm, 0.16 nm, and 0.34 nm, respectively.

To investigate the capability of the force field to describe the binding energetics, binding energies were calculated in vacuo and compared to the results obtained from DFT calculations. The results (Table S2) show that the individual vacuum binding energies obtained with the force field fall into the range of the DFT values. However, the energy difference between closed and open cages, $\Delta E(o-c)$, is slightly overestimated by the force field. The binding energy of the outside bound state is slightly underestimated by the force field by about 10 - 20 %. Nevertheless, taken together, we conclude that the force field derived in this work can provide a realistic description of this host-guest system both in terms of structure and energetics.

Table S2: Binding energies (in kcal/mol) obtained from single point energy calculations of PM6 optimized structures with different DFT functionals. For the force field energy calculations, the structures were optimized with the force field by conjugate gradient energy minimization until machine precision using GROMACS compiled in double precision. Vac: calculation performed in vacuum, disp: calculation performed with D3 dispersion correction, solv: calculation performed with polarizable continuum solvation model for acetonitrile (using the default SCRF settings in GAUSSIAN 09). All FF calculations were done in vacuum.

inside bound guest			Open cage (4O)		Closed cage (4C)		$\Delta E(4O-4C)$	
			DFT	FF	DFT	FF	DFT	FF
B3LYP	vac	6-31G*	-336.4	-362.3	-304.0	-317.6	-32.3	-44.7
		6-311G*	-336.0		-302.7		-34.3	
	vac disp	6-31G*	-377.4		-343.2		-34.1	
	solv	6-31G*	4.8		29.3		-24.5	
	solv disp	6-31G*	-36.1		-9.7		-26.4	
M06-2X	vac	6-31G*	-360.0		-330.5		-29.5	
	vac disp	6-31G*	-401.0		-369.6		-31.3	
PBE1PBE	vac	6-31G*	-345.0		-312.1		-31.9	
	vac disp	6-31G*	-386.0		-351.2		-34.7	
outside bound guest			Open cage (4O)		Closed cage (4C)		$\Delta E(4O-4C)$	
			DFT	FF	DFT	FF	DFT	FF
B3LYP	vac	6-31G*	-292.4	-261.0	-298.0	-278.0	5.6	17.0
		6-311G*	-292.0		-296.9		4.9	
	vac disp	6-31G*	-307.9		-316.4		8.5	
	solv	6-31G*	3.4		1.0		2.4	
	solv disp	6-31G*	-12.1		-17.4		5.3	
M06-2X	vac	6-31G*	-299.8		-305.6		5.8	
	vac disp	6-31G*	-315.3		-324.0		8.7	
PBE1PBE	vac	6-31G*	-293.2		-300.0		6.8	
	vac disp	6-31G*	-308.7		-318.3		9.6	

2. Bootstrapping error estimation for the PMFs

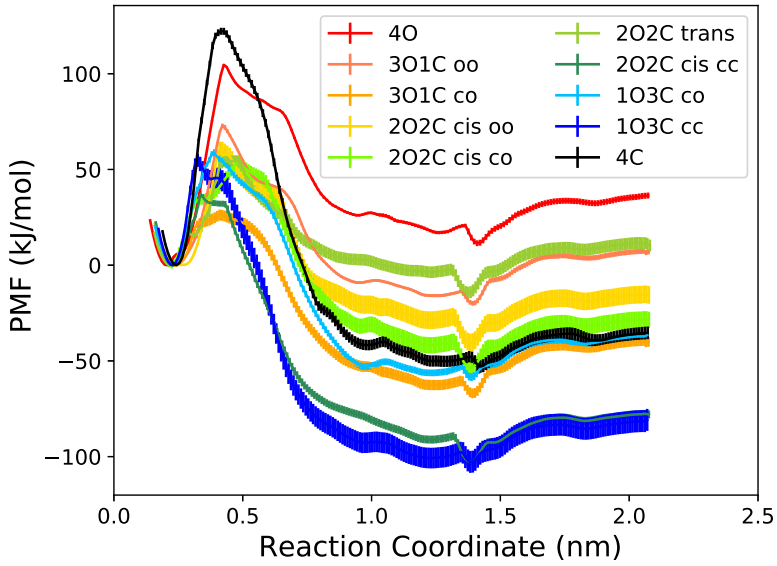

Figure S5: PMFs of all photoisomeric forms of the cage plotted with error bars obtained from Bayesian bootstrapping. 100 bootstraps were performed for each PMF.

3. Orientation restraints

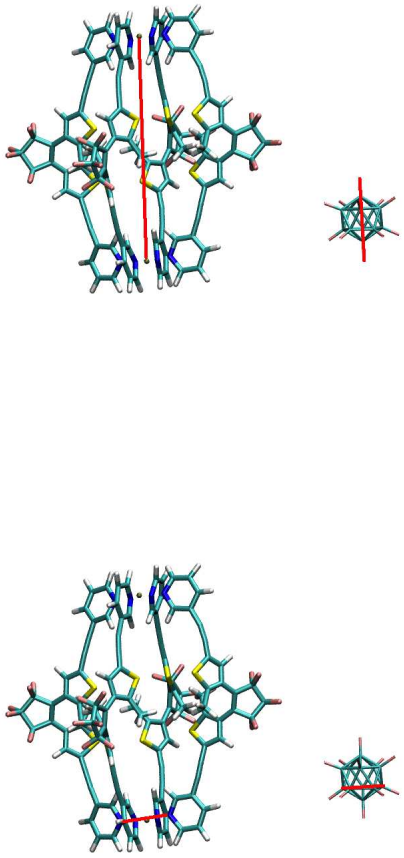

Figure S6: Illustration of the vectors used for the angle restraints applied to fix the guest in one orientation relative to the cage during the umbrella sampling simulations.

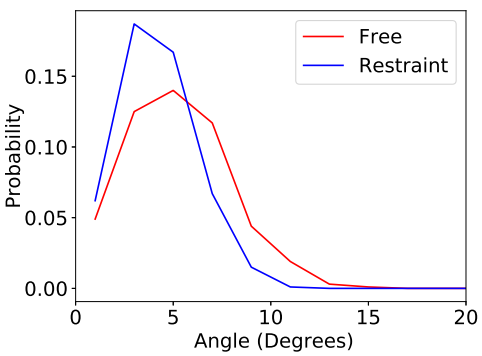

a) Open cage, guest bound

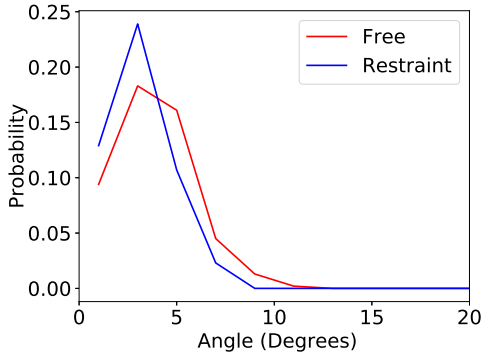

b) Closed cage, guest bound

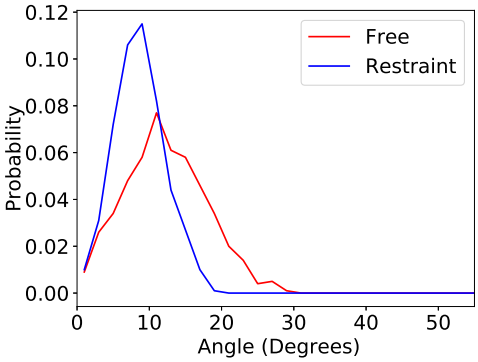

c) Open cage, guest bound

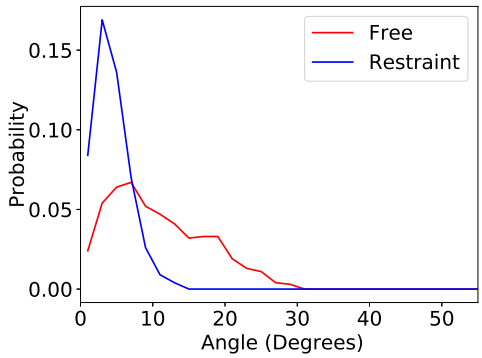

d) Closed cage, guest bound

Figure S7: Upper panel: Histograms of the angle between the Pd-Pd vector in the cage and the F-F vector in the guest (Figure S6, upper panel). Lower panel: Histograms of the angle between the N-N vector in the cage and the B-B vector in the guest (Figure S6, lower panel). The distributions were obtained from 1 ns simulations both with (blue curves) and without (red curves) the angle restraints. The angle restraints do not significantly perturb the bound state distributions.

4. Long range electrostatics cutoff

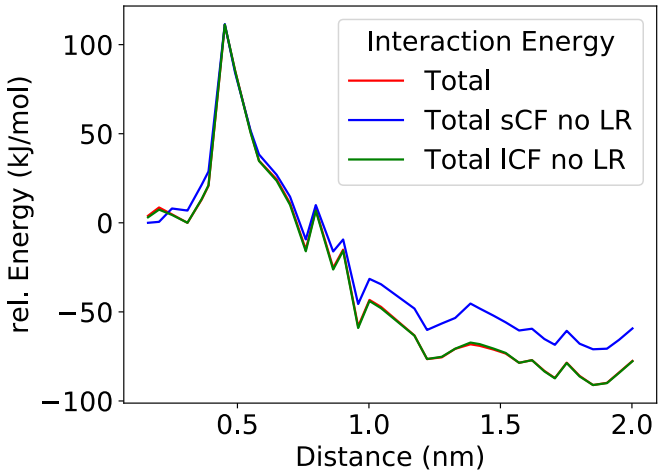

Figure S8: Interaction energy calculated for the simulation of the open cage with a nonbonded cutoffs of 1.0 nm (sCF, blue curve) and 2.4 nm (lCF, green curve). The total interaction energy (red curve) includes all contributions whereas the two curves labeled "no LR" do not include the Coulomb contributions from the PME grid part. Using a long 2.4 nm cutoff for the Lennard-Jones (6,12) interactions and to switch between real and reciprocal space for the Coulomb interactions thus quantitatively captures the interaction energies.

5. Histograms from umbrella sampling

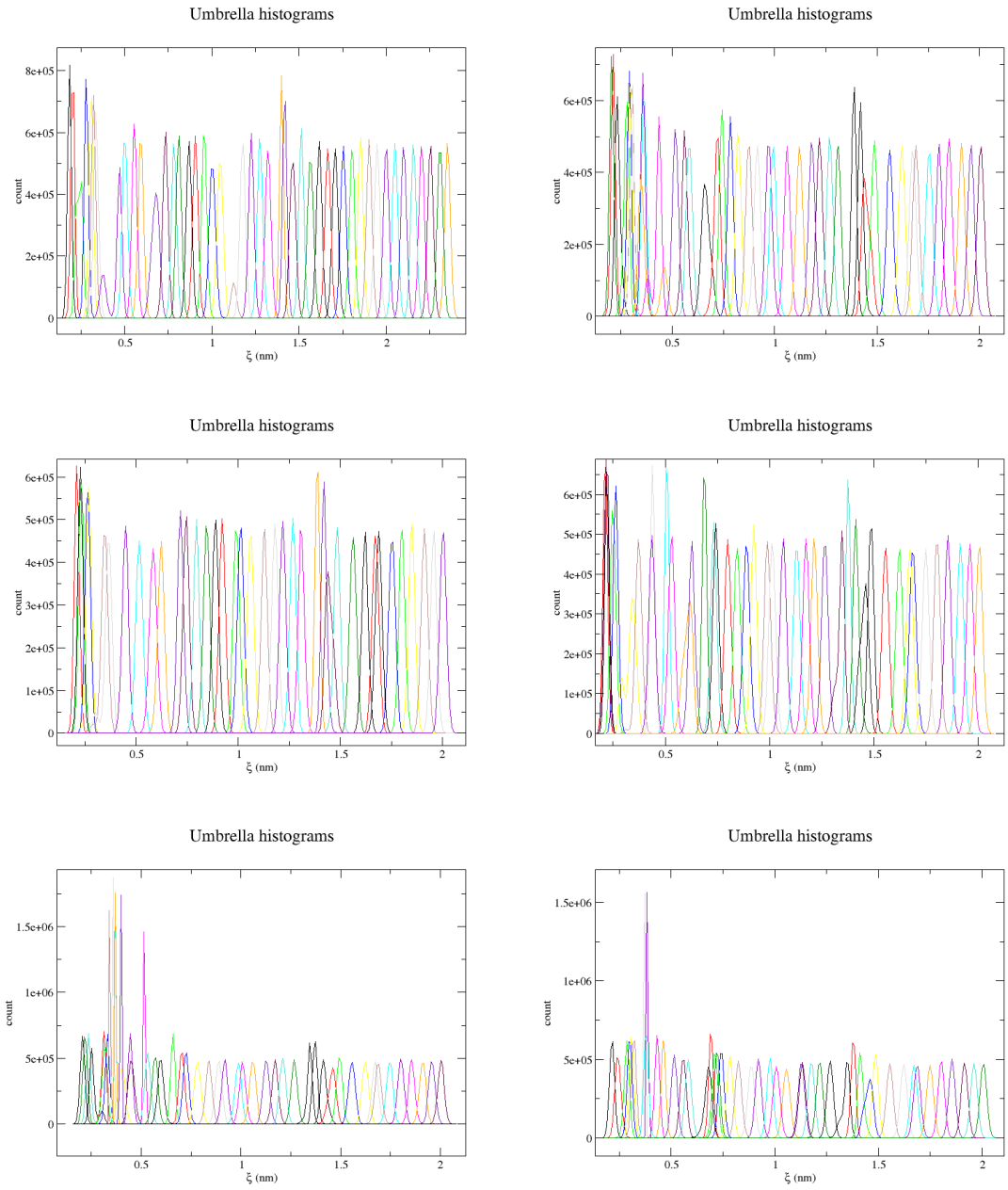

Figure S9: Histograms from the umbrella windows of the 4O (upper left), 3O1C oo (upper right), 3O1C co (middle left), 2O2C cis co (middle right), 2O2C trans (lower left), and 2O2C cis oo (lower right) simulations. The sharper histograms result from simulations performed with an umbrella force constant of 20000 kJ mol^{-1} nm^{-2}.

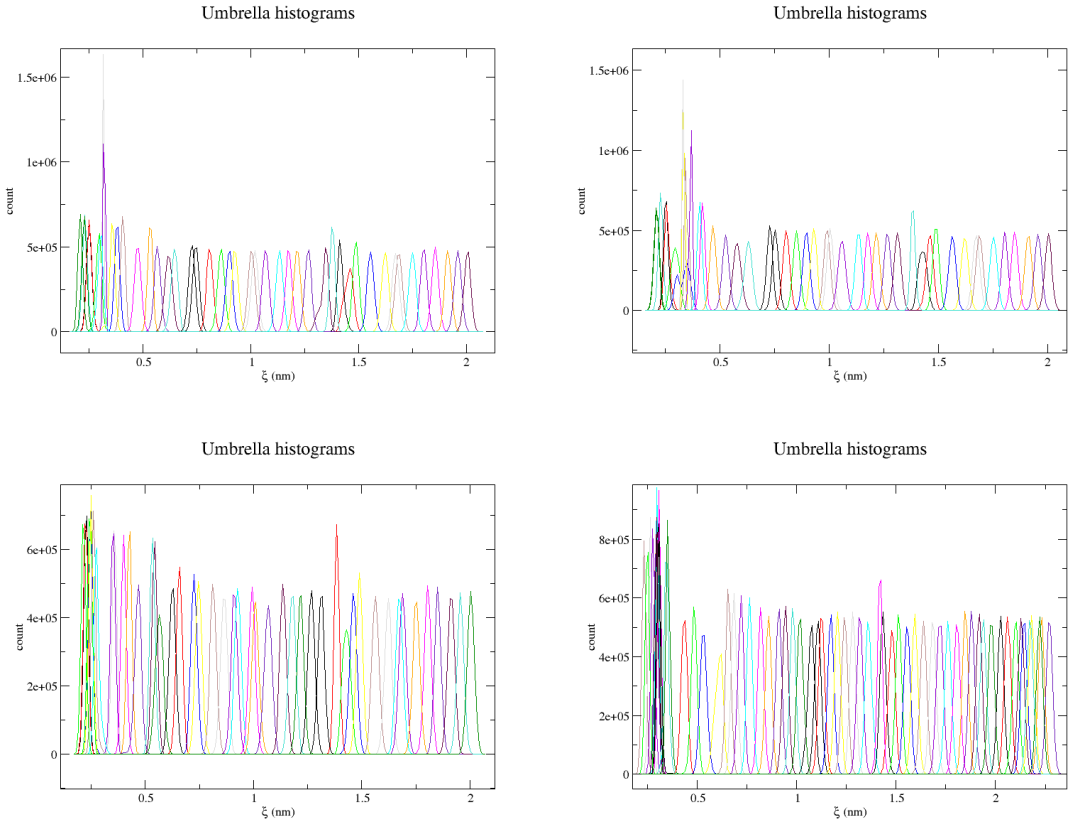

Figure S10: Histograms from the umbrella windows of 2O2C cis cc (upper left), 1O3C co (upper right), 1O3C cc (middle left), and 4C (middle right) simulations. The sharper histograms result from simulations performed with an umbrella force constant of 20000 kJ mol^{-1} nm^{-2} (upper) or 10000 kJ mol^{-1} nm^{-2} (lower).

6. Cage geometry

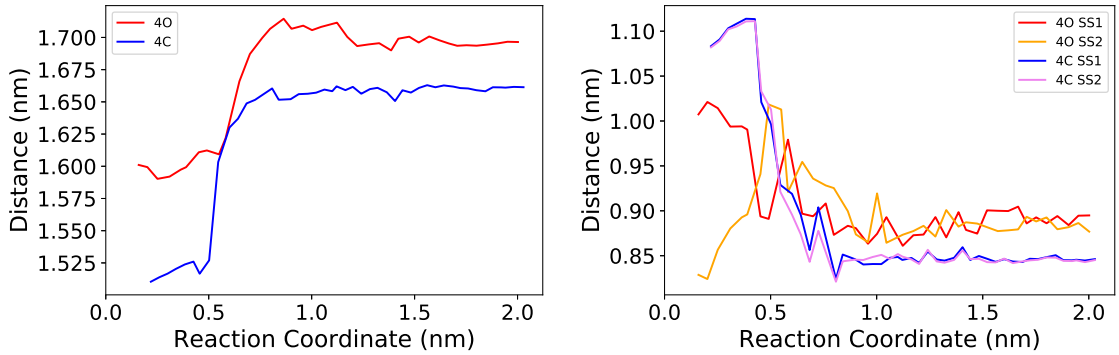

Figure S11: Pd-Pd distance (left panel) and distance between sulfur atoms (right panel) of two trans DTE ligands in the open cage (4O) and in the closed cage (4C). "Upper" and "lower" S-S distance (SS1 and SS2, respectively) refers to the distances between diagonally arranged S-atoms belonging to the "upper" and "lower" halves of the cage, that is, closer to the one or to the other Pd centre. For the open cage (4O), SS1 and SS2 are different in the bound state because the guest is slightly offset from the centre of mass of the cage (see Figure 4 in main text). This is also the case for the closed cage (4C); however, for the more rigid closed cage guest binding does not lead to differences between SS1 and SS2.

7. Solvent RDFs

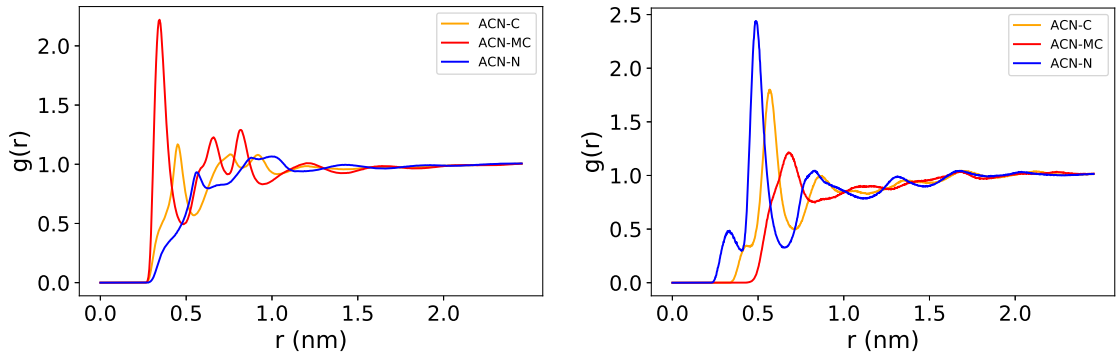

Figure S12: Radial distribution functions of acetonitrile around the fluoride atoms of the $B_{12}F_{12}^{2-}$ guest in the unbound state (left panel), and around the Pd centers of the cage in the unbound state (right panel). The methyl-carbon (ACN-MC), central carbon (ACN-C), and nitrogen atom (ACN-N) of acetonitrile were analysed separately.